

Article

Theoretical Study of the Multiferroic Properties of Ion-Doped $\text{CaBaCo}_4\text{O}_7$

Iliana N. Apostolova ¹, Angel T. Apostolov ² and Julia M. Wesselinowa ^{3,*}¹ University of Forestry, Kl. Ohridsky Blvd. 10, 1756 Sofia, Bulgaria; inaapos@abv.bg² University of Architecture, Civil Engineering and Geodesy, Hr. Smirnenski Blvd. 1, 1046 Sofia, Bulgaria; angelapos@abv.bg³ Faculty of Physics, Sofia University "St. Kliment Ohridski", J. Bouchier Blvd. 5, 1164 Sofia, Bulgaria

* Correspondence: julia@phys.uni-sofia.bg

Abstract: Using a microscopic model and Green's function theory, we investigated the magnetization, specific heat, and polarization properties of $\text{CaBaCo}_4\text{O}_7$ (CBCO), scrutinizing their variations with temperature, magnetic field strength, and doping effects. Our analysis revealed a conspicuous kink in the specific heat curve near the critical temperature (T_C), indicative of a phase transition. Additionally, the observed increase in polarization, P with escalating magnetic field strength serves as compelling evidence for the multiferroic nature of CBCO. Substituting Co ions with Fe ions resulted in an augmentation of the CBCO magnetization, M , while doping with Zn, Mn, or Ni ions led to a decline. Similarly, doping CBCO with Y or Sr ions at the Ca site exhibited divergent effects on magnetization, M , with an increase in the former and a decrease in the latter case. This modulation of the magnetization, M , can be attributed to the varying strains induced by the doping ions, thereby altering the exchange interaction constants within the system. The polarization, P , increases by Ni, Mn, or Zn substitution on the kagome layer Co sites. It can be concluded that Ni, Mn, or Zn doping enhances the magnetoelectric effect of CBCO. Notably, our findings align qualitatively well with experimental observations, reinforcing the validity of our theoretical framework.

Keywords: $\text{CaBaCo}_4\text{O}_7$; ion doping; magnetization; specific heat; polarization; microscopic model; green's function theory



Citation: Apostolova, I.N.; Apostolov, A.T.; Wesselinowa, J.M. Theoretical Study of the Multiferroic Properties of Ion-Doped $\text{CaBaCo}_4\text{O}_7$. *Appl. Sci.* **2024**, *14*, 4859. <https://doi.org/10.3390/app14114859>

Academic Editor: Young-Min Kim

Received: 29 April 2024

Revised: 1 June 2024

Accepted: 3 June 2024

Published: 4 June 2024



Copyright: © 2024 by the authors. Licensee MDPI, Basel, Switzerland. This article is an open access article distributed under the terms and conditions of the Creative Commons Attribution (CC BY) license (<https://creativecommons.org/licenses/by/4.0/>).

1. Introduction

$\text{CaBaCo}_4\text{O}_7$ (CBCO) is a new type of ferrimagnet composed entirely of CoO_4 tetrahedra. This structure is similar to other members of the "114" series, such as $\text{LnBaCo}_4\text{O}_7$, featuring alternating kagome and triangular layers. The first kagome magnet that was found to exhibit zero-field magnetism at room temperature was the intermetallic compound Fe_3Sn_2 , as reported by Kida in 2011 [1]. Kagome magnets can have various crystal and magnetic structures, typically containing a $3d$ -transition-metal kagome lattice. Examples include the antiferromagnet Mn_3Sn , the paramagnet CoSn , the ferrimagnet TbMn_6Sn_6 , the ferromagnet $\text{Co}_3\text{Sn}_2\text{S}_2$, Fe_3Sn_2 , Co_2MnGa , and the magnetic class AV_3Sb_5 (where $A = \text{Cs, Rb, K}$). $\text{CaBaCo}_4\text{O}_7$ (CBCO) has garnered significant attention owing to its initial exploration of charge ordering phenomena among Co^{2+} and Co^{3+} ions. This compound exhibits an orthorhombic distortion [2–6], a phenomenon well-documented in previous studies, which alleviates geometric magnetic frustration evident in both its kagome and triangular layers. Below its magnetic transition temperature (T_C) at 70 K, CBCO manifests a remarkably substantial spin-induced polarization, indicative of a significant ferrimagnetic moment, thereby suggesting the potential for magnetic control over electric polarization [7–11]. Notably, research conducted by Fishman et al. [12] underscores the intricate interplay of competing exchange interactions on alternating triangular and kagome layers within CBCO, resulting in complex magnetic states and spin-induced electric polarizations below the critical temperature (T_C). While CBCO exhibits an inaccessible ferroelectric transition

and lacks switchable permanent electric polarization [9], its application prospects remain promising, particularly in harnessing the substantial spin-induced polarization facilitated by a magnetic field slightly below T_C [7].

Multiferroics are materials that exhibit more than one primary ferroic property within the same phase, such as ferromagnetism, ferroelectricity, and ferroelasticity [13]. In magneto-electric materials, an electric field can influence the magnetic properties and vice versa. A material is considered ferroelectric if it has a spontaneous electric polarization that can be switched by an applied electric field. This electric polarization typically results from a structural distortion that breaks inversion symmetry from a parent centrosymmetric phase, as seen in BaTiO₃. In lone-pair-active multiferroics, the ferroelectric displacement is driven by the A-site cation, while magnetism arises from a partially filled d shell on the B site, exemplified by BiFeO₃. Geometric ferroelectrics achieve a polar ferroelectric state through rotational distortion of the polyhedra, which drives the structural phase transition. In magnetically driven multiferroics, long-range non-centrosymmetric magnetic order induces macroscopic electric polarization. There are two categories of multiferroics: type I, where magnetism and ferroelectricity have separate origins, and type II, where ferroelectricity stems from the system's internal magnetism. Multiferroic materials have applications in actuators, switches, magnetic field sensors, new types of electronic memory devices, and nonvolatile memory.

Additionally, the properties of ion-doped CBCO can be finely adjusted through doping with elements such as Zn, Y, Ni, Fe, and Al at the Co site [11,14–24]. Neutron powder diffraction analyses of Zn-doped CBCO have revealed a reduction in the strength of magnetic interactions between the bitetrahedral cobalt c -axis chains, accompanied by a lowering of the ferrimagnetic transition temperature from 60 to 55 K [14]. Intriguingly, this doping-induced alteration also results in a discernible switching of electric polarization [14]. Gen et al. [16] have documented a notable enhancement in the magnitude of magnetic field-induced electric polarization in Ni-doped CBCO. Additionally, Sarkar et al. [17] observed a reduction in the ferrimagnetic transition temperature of CBCO from 60 to 55 K upon Zn substitution. Oda et al. [18] delved into the effects of impurity substitution on the magnetoelectric properties of CBCO, revealing that increasing Fe doping results in a downward shift of the transition temperatures for both the ferrimagnetic- and ferroelectric-like phases. Notably, Y-doped CBCO at the Ca site exhibited magnetic properties and ferrimagnetism persisting up to a critical temperature (T_C) of 270 K [25]. Conversely, the replacement of Sr for Ba in CBCO disrupts its ferrimagnetic behavior due to the intense competition between long-range ferrimagnetic ordering and magnetic frustration [26].

The investigation of undoped CBCO properties through theoretical approaches remains relatively limited. Johnson et al. [9] conducted ab initio calculations coupled with the Landau theory to explore magneto-electric coupling in CBCO, while Fishman et al. [12] proposed a microscopic model that accounts for exchange interactions among Co ions and various anisotropies to elucidate the ferrimagnetic and multiferroic characteristics of CBCO. These studies contribute significantly to understanding the complex behavior of CBCO, shedding light on its intriguing physical phenomena.

Our paper aims to explore the multiferroic attributes of both undoped and ion-doped CBCO, utilizing a microscopic model and Green's function theory, an approach that, to our understanding, has not been previously explored in existing literature. Let us mention that the polar magnet CBCO is known to exhibit the largest magnetic-field-driven electric polarization change, which has important technological applications. Moreover, ion doping changes its properties, leading to the enhancement of magnetoelectric coupling.

2. The Model

The Hamiltonian describing the multiferroic properties of CBCO is as follows:

$$H = H_m + H_f + H_{mf}. \quad (1)$$

Fishman et al. [12] proposed a Heisenberg model for the magnetic properties of pure CBCO with 12 nearest-neighbor interactions and associated anisotropies. The magnetic state of CBCO can be described as a triangular array of ferrimagnetically aligned, bitetrahedral *c*-axis chains with net moment along *b* (see Figure 1). Competing interactions within each chain produce a non-collinear spin state. Each magnetic unit cell of CBCO contains 16 Co ions on two kagome layers and two triangular layers. Moreover, the cobalt atoms can be either in a fluctuating Co²⁺/Co³⁺ valence state or Co²⁺ and Co³⁺ ions. We extend this model here in order to study the magnetic properties of ion-doped CBCO:

$$\begin{aligned}
 H_m = & -\frac{1}{2} \sum_{i,j} (1-x) J_{ij}^{Co-Co} \mathbf{S}_i^{Co} \cdot \mathbf{S}_j^{Co} - \frac{1}{2} \sum_{i,k} x J_{i,k}^{Co-DI} \mathbf{S}_i^{Co} \cdot \mathbf{S}_k^{DI} \\
 & + D^{kag} \sum_{i,kag} S_{ic}^2 + D^{tri} \sum_{i,tri} S_{ic}^2 - C^{kag} \sum_{i,kag} (\mathbf{o}_i \cdot \mathbf{S}_i)^2 \\
 & - C^{tri} \sum_{i,tri} (\mathbf{n}_i \cdot \mathbf{S}_i)^2 - g\mu_B \mathbf{h} \cdot \sum_i \mathbf{S}_i^{Co},
 \end{aligned} \tag{2}$$

where \mathbf{S}_i is the Heisenberg spin operator of the Co spin at the site i ; J is the exchange interaction constant between the Co-Co or Co-doping ions (DI); x is the ion doping concentration. Six of these exchange interaction constants (J_1 – J_6) couple the kagome and triangular layers as shown in Figure 1; the other six exchange interaction constants (J_7 – J_{12}) couple the spins within a kagome layer. D and C are easy-plane and easy-axis anisotropy constants, whereas \mathbf{o}_i and \mathbf{n}_i are the unit vectors for the kagome and triangular layers, respectively [12]. The hexagonal anisotropy can be neglected, it is very small. \mathbf{h} is an external magnetic field.

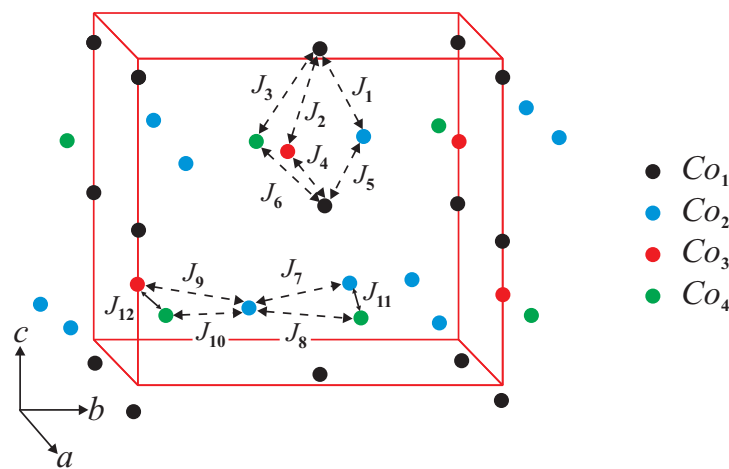


Figure 1. Structure of the elementary cell of CBCO with the 12 nearest-neighbor spin interactions, 6 of which (J_1 through J_6) couple the kagome and triangular layers, the other 6 (J_7 through J_{12}) couple the spins within a kagome layer.

Below the ferrimagnetic transition, CBCO is reported to develop a very large spin-induced polarization, P , which classifies it as a type I multiferroic. This polarization must be generated by the dependence of the exchange interactions J_{ij} on an electric field, called magnetostriction. The electric polarization, P , produced between two magnetic moments is given by the following:

$$\mathbf{P} = a \sum_{ij} \mathbf{e}_{ij} \times (\mathbf{S}_i \times \mathbf{S}_j). \tag{3}$$

\mathbf{e}_{ij} is the unit vector connecting the sites i and j . The proportional constant a is determined by the spin exchange and spin-orbit interactions [27,28].

An orthorhombic distortion above the phase transition temperature (T_C) partially relieves the geometric frustration on the kagome and triangular layers and allows ferrimag-

netism and ferroelectricity to coexist below T_C in CBCO. Although occupying a triangular lattice, bitetrahedral c -axis chains are ferrimagnetically ordered in the ab plane. Competing interactions within each chain produce non-collinear spin states. Sets of bonds coupling those chains are responsible for the large spin-induced polarization of CBCO. The magnetoelectric coupling is taken to be linear [9] due to the coincidence between the magnetic and ferroelectric phase transition temperatures:

$$H_{mf} = -g \sum_{ikl} P_i M_k M_l. \tag{4}$$

g is the magnetoelectric coupling constant.

The spontaneous magnetization, M , of CBCO is as follows:

$$M = | M_A + M_B |. \tag{5}$$

M_A and M_B are the magnetizations of the kagome and triangular layers, respectively, which are calculated from the following:

$$M^{A,B} = \langle S^z \rangle^{A,B} = \frac{1}{N} \sum_i \left[(S + 0.5) \coth[(S + 0.5)\beta E_{mi}^{A,B}] - 0.5 \coth(0.5\beta E_{mi}^{A,B}) \right], \tag{6}$$

where $\beta = 1/k_B T$, k_B is the Boltzmann constant, T is the absolute temperature, $E_{mi}^{A,B}$ is the spin-wave energy of the two layers, calculated using the matrix Green's function for the magnetic subsystem:

$$g_{ij} = \langle\langle S_i^{+A,B}; S_j^{-A,B} \rangle\rangle. \tag{7}$$

3. Theoretical Method

For the approximate calculation of the Green's function, we use a method proposed by Tserkovnikov [29]. It goes beyond the random phase approximation, taking into account all correlation functions. Moreover, this method also allows us to calculate the imaginary part of the Green's function. We will now briefly sketch this method. After a formal integration of the equation of motion for the retarding two-time Green's function, i.e.,

$$g_{ij}(t) = \langle\langle S_i^+(t); S_j^- \rangle\rangle \tag{8}$$

one obtains

$$g_{ij}(t) = -i\theta(t)\langle[S_i^+; S_j^-]\rangle \exp(-iE_{ij}(t)t), \tag{9}$$

with $\theta(x) = 1$ for $x > 0$, $\theta(x) = 0$ for $x < 0$,

$$E_{ij}(t) = \omega_{ij} - \frac{i}{t} \int_0^t dt' t' \left(\frac{\langle[j_i(t); j_j^+(t')]\rangle}{\langle[S_i^+(t); S_j^-(t')]\rangle} - \frac{\langle[j_i(t); S_j^-(t')]\rangle \langle[S_i^+(t); j_j^+(t')]\rangle}{\langle[S_i^+(t); S_j^-(t')]\rangle^2} \right) \tag{10}$$

and $j_i(t) = \langle[S_i^+(t), H_{interaction}]\rangle$. The time-independent term

$$E_{ij} = \frac{\langle[[S_i^+, H]; S_j^-]\rangle}{\langle[S_i^+; S_j^-]\rangle} \tag{11}$$

is the excitation energy in the generalized Hartree–Fock approximation. The time-dependent term in Equation (10) includes damping effects.

Another theoretical method is density functional theory (DFT), which is a powerful tool for investigating many-body problems. However, DFT is mostly concerned with

ground state properties at zero temperature, whereas we can make a finite temperature analysis of the excitation spectrum and all physical quantities. Whereas within DFT, all parameters of the system can be—at least in principle—calculated, and we are forced to use additional models to find out those parameters. We are convinced that both approaches, DFT and the Green’s function method, are well-suited and, to a certain extent, alternative methods for describing many-body systems.

4. Numerical Results and Discussion

The numerical calculations are performed in the JAVA programming environment using simple iterative procedures and summation over nearest neighbors. For the numerical calculations of the properties of CBCO, the following model parameters are used: $J_1 = J_5 = -92$ meV, $J_3 = J_6 = 41$ meV, and $J_8 = 188$ meV lie within connected bitetrahedral *c*-axis chains, whereas $J_{10} = 108$ meV couples two chains, and lies between nearly parallel spins, $D^{kag} = -0.67$ meV, $D^{tri} = -1.24$ meV, $C^{kag} = 3.7$ meV, $C^{tri} = 0.77$ [12], $g = 0.1$ eV.

4.1. Temperature Dependence of the Magnetization of CBCO

Initially, we undertake an analysis of the temperature-dependent behavior of the magnetization, M , along the *b*-axis, utilizing Equation (5) from the CBCO framework. The resulting depiction, as illustrated in Figure 2, is found to be consistent with empirical observations from various experimental sources [3,6,9,17,18]. Notably, a pronounced reduction is observed around the critical temperature (T_C) = 70 K, aligning with theoretical expectations (denoted as curve 1). Furthermore, the magnetization values at lower temperatures provide compelling evidence supporting the presence of charge ordering among the Co ions. Upon the application of an external magnetic field, h , both the magnetization, M , and the critical temperature (T_C) demonstrate an increase (denoted as curve 2), thereby elucidating the influence of external perturbations on the magnetic properties of the system. The magnetic field, h , tries to arrange the spins in its direction. Thus, it increases those that are parallel to its direction or rotates those that are in the opposite direction. The final effect is an increase in the magnetization, M . When the external magnetic field, h , is absent, there is a second-order phase transition in the system, and the magnetization, M , vanishes at the critical magnetic phase transition temperature because there is a discontinuity in the magnetic susceptibility vs. temperature T (not shown here). When the external magnetic field, h , is non-zero, the magnetic susceptibility vs. T is now continuous. The phase transition is broader.

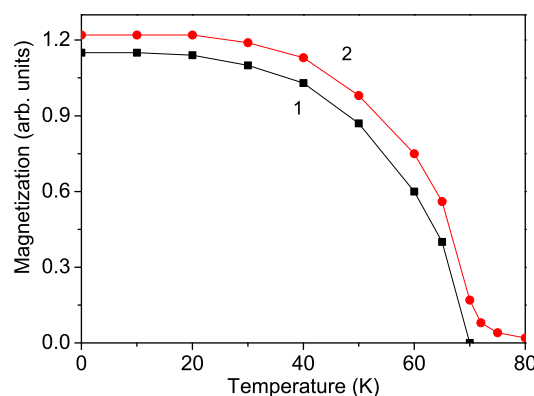


Figure 2. Temperature dependence of the magnetization, M , of CBCO for different magnetic field, h , values: (1) 0, (2) 1 kOe.

4.2. Temperature and Magnetic Field Dependence of the Specific Heat in CBCO

In the context of Figure 3, curve 1 depicts the specific heat C_p of CBCO as a function of temperature T for zero magnetic field, $h = 0$, determined through the derivative $C_p = d\langle H \rangle / dT$, where H represents the comprehensive Hamiltonian. Notably, a discernible

anomaly appears in the curve near the critical temperature (T_C) = 70 K, a phenomenon consistently observed in studies by Caignaert et al. [3], Oda et al. [18], and Iwamoto et al. [6]. Upon the imposition of an external magnetic field, h , the specific heat, C_p , increases. Moreover, for weak magnetic fields, the peak becomes smaller, wider, and shifts to higher temperature values, whereas for strong magnetic fields, it disappears, as depicted in Figure 3, curves 2 and 3.

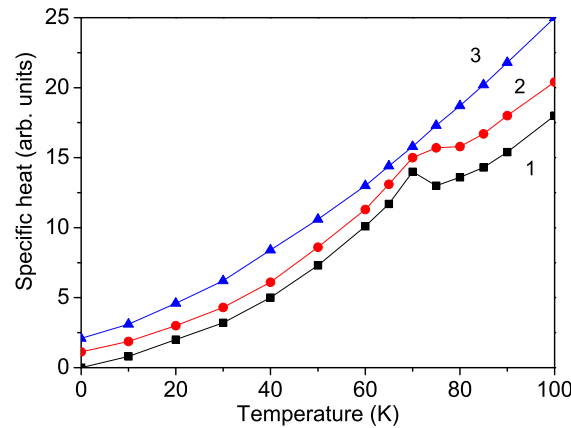


Figure 3. Temperature dependence of the specific heat C_p of CBCO for different magnetic field, h , values: (1) 0, (2) 1, (3) 10 kOe.

4.3. Temperature and Magnetic Field Dependence of the Polarization in CBCO

The strong electric polarization, P , of CBCO below the critical temperature (T_C) is induced by the displacement of oxygen atoms surrounding bonds that couple the triangular and kagome layers. The calculation of the spin-induced polarization, P , along the c -axis in CBCO is derived from Equation (3), with the resulting data presented in Figure 4. Notably, the polarization, P , exhibits a diminishing trend with rising temperature, T , ultimately reaching nullity at the critical ferrimagnetic temperature (T_C) = 70 K. Additionally, augmentation of polarization is observed with the increasing magnetic field, h , as illustrated in the inset of Figure 4, providing compelling evidence for the multiferroic nature of CBCO. This observation aligns with the findings by Johnson et al. [9] and Iwamoto et al. [6], who similarly reported an enhanced polarization, P , in response to the external magnetic field, h . A peak around the ferrimagnetic phase transition temperature (T_C) is reported in the dielectric constant ϵ along the c axis in CBCO [6,18,24], which is also evidence for the multiferroic behavior of CBCO.

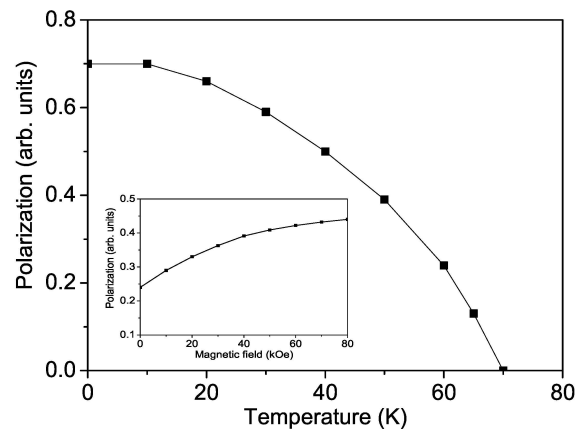


Figure 4. Temperature dependence of the polarization, P , of CBCO. Inset: Magnetic field dependence of the polarization, P , of CBCO for $T = 60$ K.

4.4. Dependence of the Magnetization in CBCO on the Dopant Concentration at the Co Site

The primary objective of this study is to explore the influence of doping on the multiferroic characteristics of the CBCO compound. It is important to note that the exchange interaction constant J is intricately linked to the spatial arrangement of spins, relying on lattice parameters, lattice symmetry, and the number of nearest neighbors, while also being susceptible to various strains. Specifically, J is inversely proportional to the distance separating adjacent spins within the lattice. Doping introduces a disparity in ionic radii between the dopant and the host Co ions, thereby inducing strain. In scenarios where the doping ion possesses a larger ionic radius, tensile strain ensues, leading to an expansion of lattice parameters and a consequent reduction in the exchange interaction constant under doping, denoted as J_d , $J_d < J$. Conversely, when a compressive strain occurs due to a smaller dopant ionic radius, lattice parameters contract, increasing J_d , $J_d > J$.

The influence of the doping concentration is quantified through the factors $(1 - x)$ and x in the first two terms of Equation (1), respectively. Here, x represents the doping concentration, wherein the exchange interaction constant J progressively diminishes from its maximal value in the absence of doping ($x = 0$) to the exchange interaction constant J_d in the scenario where all host ions are replaced by dopants ($x = 1$).

Initially, our investigation focuses on the substitution of Fe into the Co site of CBCO. The Fe atoms preferentially occupy the sites at the triangular layer as shown by Cuartero et al. [30]. Given that the ionic radius of the Fe dopant exceeds that of the host Co ion, inducing tensile strain, we anticipate the relation $J_d < J$. This strain-induced modulation is reflected in the observed enhancement of magnetization, M , with increasing Fe dopant concentration x , as depicted in Figure 5, curve 1. This trend is consistent with observations reported by Oda et al. [18] and Seikh et al. [11].

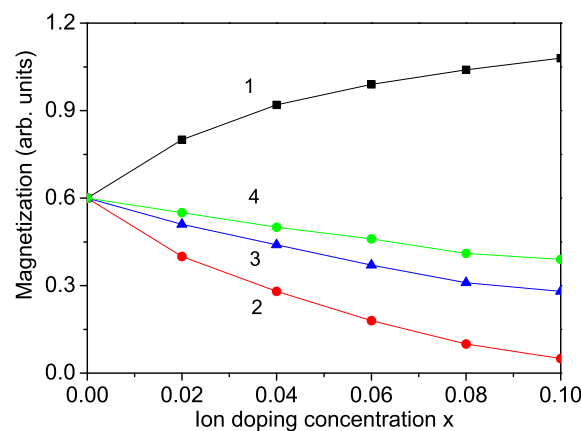


Figure 5. Dependence of the magnetization on the dopant concentration x of CBCO for different doping ions: (1) Fe, (2) Zn, (3) Mn, (4) Ni.

We calculated the Fe doping dependence of the specific heat C_p . The results are shown in Figure 6. It can be seen that C_p increases with increasing x . There is also a peak at T_C , which is shifted to higher T values because T_C is enhanced for larger x values. The results are in agreement with the experimental data of Oda et al. [18].

Continuing our investigation, we turn our attention to Zn as a doping ion within CBCO. The Zn atoms prefer occupying the kagome layer as shown by Cuartero et al. [30]. Given the larger ionic radius of the Zn^{2+} ion (0.88 Å) compared to that of Co^{2+} one (0.79 Å), i.e., a tensile strain arises, necessitating the application of the relationship $J_d > J$. Consequently, this strain-induced effect manifests as a reduction in magnetization, M , as depicted in Figure 5, curve 2, aligning closely with the experimental findings by Sarkar et al. [17], Sekhar et al. [14], and Cuartero et al. [30]. Notably, for higher Zn doping concentrations x , such as $x = 3$, the magnetization, M , reaches a critical point of vanishing, indicative of a transition from ferrimagnetic CBCO to antiferromagnetic Zn-doped CBCO. Further-

more, similar reductions in the magnetization, M , are observed upon ion doping with Ni ($r = 0.83 \text{ \AA}$) or Mn ($r = 0.81 \text{ \AA}$), both possessing larger radii than Co ions, thereby inducing tensile strain. This corroborates with the findings depicted in Figure 5, curves 3 and 4, as reported by Wang et al. [31], Gen et al. [16], and Sekhar et al. [32], indicating a weakening of ferrimagnetic interactions upon Mn doping, and a decrease in the magnetization, M , upon Ni doping.

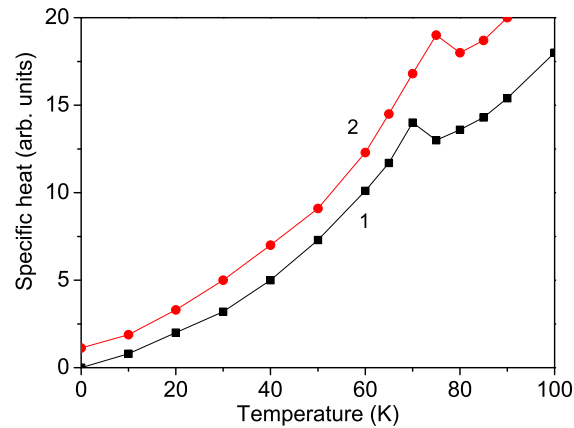


Figure 6. Temperature dependence of the specific heat C_p of CBCO for different Fe dopant concentrations x : (1) $x = 0$, (2) 0.1.

4.5. Dependence of the Magnetization in CBCO on the Dopant Concentration at the Ca Site

It is worth mentioning that ion substitution can also occur at the Ca sites within CBCO, which is a topic that we will briefly address. The ionic radius of the Ca^{2+} ion is 1.14 \AA , and when doped with ions such as Y^{3+} ($r = 1.04 \text{ \AA}$) or Sr^{2+} ($r = 1.18 \text{ \AA}$), different strain effects emerge. Specifically, when Y is substituted, resulting in a smaller ionic radius than that of Ca, a compressive strain (where $J_d > J$) ensues, whereas with Sr doping, which possesses a larger radius than Ca, a tensile strain (where $J_d < J$) arises. Consequently, within our model, Y doping at the Ca site is anticipated to enhance magnetization, M , while Sr doping is expected to reduce M , aligning with experimental observations by Raveau et al. [25] and Seikh et al. [26], respectively. These predictions are illustrated in Figure 7, curves 1 and 2. Additionally, it is noteworthy that the extent of magnetization modification resulting from Ca site substitution is comparatively smaller than that observed with Co site substitution.

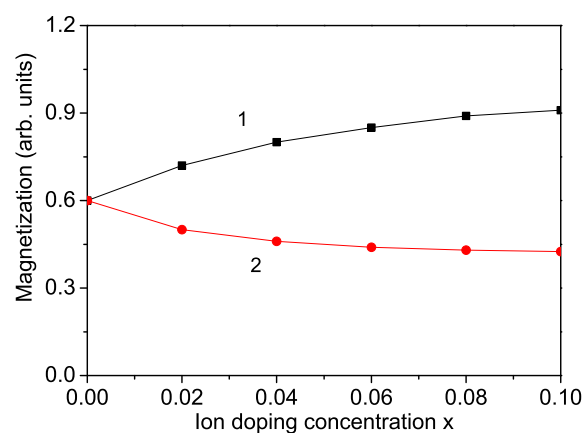


Figure 7. Dependence of the magnetization on the dopant concentration x of CBCO for different doping ions at the Ca site: (1) Y, (2) Sr.

4.6. Dependence of the Polarization in CBCO on the Dopant Concentration at the Co Site

In our final analysis, we delve into the effects of doping, exemplified by Ni or Zn, on the polarization, P , within CBCO. Substitution of magnetic Ni ions at kagome layer Co sites within CBCO results in an augmentation of polarization, P , as illustrated in Figure 8, curve 1, a trend corroborated by findings from Gen et al. [16] and Zhou et al. [24]. Fishman et al. [12] have elucidated that the ordering of Co charges and the configuration of exchange bonds within the kagome layer play pivotal roles in inducing significant spin-induced electric polarization, P . Moreover, the spin structure within the kagome layer undergoes a transition from non-collinear to collinear (up-up-down-down) upon Ni ion doping, accompanied by a reduction in magnetization, M , and a shift from a ferrimagnetic to an antiferromagnetic ground state, as depicted in Figure 5, curve 4. Similarly, an increase in the polarization, P , is observed with Mn ion doping in CBCO, as shown in Figure 8, curve 2, an observation recently reported by Wang et al. [31]. The enhancement of P is smaller compared to that of the Ni-doped CBCO.

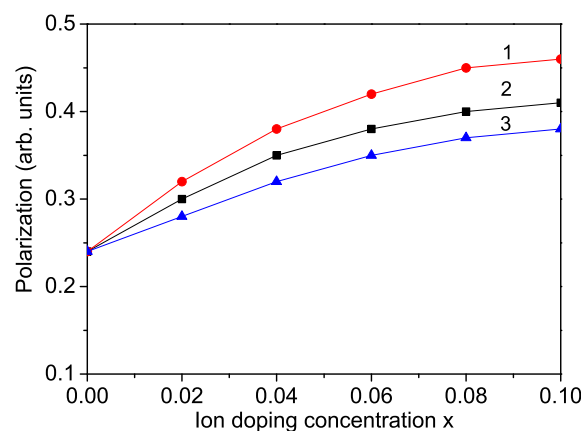


Figure 8. Dependence of the polarization on the dopant concentration x of CBCO for $T = 60$ K for different doping ions: (1) Ni, (2) Mn, (3) Zn.

Let us explore the scenario wherein nonmagnetic Zn ions are substituted for Co ions within CBCO. This substitution not only fills the Co positions within the kagome layers but also diminishes the orthorhombic distortion. Furthermore, Zn doping serves to stabilize antiferromagnetic ordering, exerting a significant influence on both the magnetic properties and the spin-induced polarization. As depicted in Figure 8, curve 3, an increase in the polarization, P , is observed with rising concentrations of nonmagnetic Zn dopant, consistent with findings reported by Sekhar et al. [14]. It is worth highlighting that the potential impacts of doping on the dielectric properties of CBCO will be explored in future research endeavors.

5. Conclusions

In summary, employing a microscopic model and Green's function technique, we conducted a comprehensive examination of the magnetization, M , specific heat C_p , and polarization, P , of CBCO, scrutinizing their dependencies on temperature, magnetic field strength, and doping effects. Notably, Fishman et al. [12] previously investigated the magnetic and electric properties of pure CBCO utilizing a modified Heisenberg model, while to the best of our knowledge, the influence of doping on the magnetic and electric properties of CBCO remains unexplored in existing literature. Our analysis reveals a distinct kink in the temperature-dependent specific heat curve near the critical temperature (T_C), indicative of a phase transition. By applying strong magnetic fields, this peak disappears. Furthermore, the observed augmentation in polarization, P , with increasing external magnetic field strength serves as compelling evidence for the multiferroic nature of CBCO. Additionally, the magnetization, M , of CBCO displays a notable increase upon substitution

of Co ions with Fe, whereas doping with Zn, Mn, or Ni ions induces a decline. Similarly, doping CBCO with Y or Sr ions at the Ca site elicits contrasting effects on magnetization, M , with an increase in the former and a decrease in the latter case, attributable to disparate strains induced by the doping ions, thereby altering the exchange interaction constants. If magnetic Ni or nonmagnetic Zn atoms occupy the kagome layer Co sites in CBCO, then the polarization, P , increases with the increasing Ni, Mn, or Zn dopant. We can conclude that Ni, Mn, or Zn doping enhances the magnetoelectric effect of CBCO. Thus, our study offers insight into the microscopic mechanisms underlying the macroscopic properties of CBCO and demonstrates qualitative agreement with experimental observations. The good agreement with many experimental data points is evidence that our model and Green's function method are suitable for describing the various properties of pure and ion-doped CBCO.

It should be mentioned that the multiferroic properties of CBCO nanoparticles, including co-doping (for example, with Fe and Zn, $\text{CaBaCo}_{4-x-y}\text{Fe}_x\text{Zn}_y\text{O}_7$ [30]) will be studied in a future article. It is an interesting case because Fe atoms preferentially substitute the Co atoms at the triangular layer whereas Zn atoms occupy the kagome layer.

Author Contributions: Conceptualization, J.M.W.; Methodology, I.N.A. and A.T.A.; Software, I.N.A.; Formal analysis, A.T.A.; Investigation, I.N.A., A.T.A. and J.M.W.; Writing—original draft, J.M.W. All authors have read and agreed to the published version of the manuscript.

Funding: This research received no external funding.

Institutional Review Board Statement: Not applicable.

Informed Consent Statement: Not applicable.

Data Availability Statement: The original contributions presented in the study are included in the article, further inquiries can be directed to the corresponding author.

Conflicts of Interest: The authors declare no conflicts of interest.

References

1. Kida, T. The giant anomalous Hall effect in the ferromagnet Fe_3Sn_2 —A frustrated kagome metal. *J. Phys. Condens. Matter.* **2011**, *23*, 112205. [[CrossRef](#)]
2. Caignaert, V.; Pralong, V.; Maignan, A.; Raveau, B. Orthorhombic kagome cobaltite $\text{CaBaCo}_4\text{O}_7$ (CBCO): A new ferrimagnet with a TC of 70 K. *Solid State Commun.* **2009**, *149*, 453–455. [[CrossRef](#)]
3. Caignaert, V.; Pralong, V.; Hardy, V.; Ritter, C.; Raveau, B. Magnetic structure of $\text{CaBaCo}_4\text{O}_7$: Lifting of geometrical frustration towards ferrimagnetism. *Phys. Rev. B* **2010**, *81*, 094417. [[CrossRef](#)]
4. Raoufi, T.; He, J.; Wang, B.; Liu, E.; Sun, Y. Magnetocaloric properties and Griffiths phase of ferrimagnetic cobaltite $\text{CaBaCo}_4\text{O}_7$. *Chin. Phys. B* **2023**, *32*, 017504. [[CrossRef](#)]
5. Qu, Z.; Ling, L.; Zhang, L.; Pi, L.; Zhan, Y. Magnetic properties of the ferrimagnetic cobaltite $\text{CaBaCo}_4\text{O}_7$. *Solid State Commun.* **2011**, *151*, 917–919. [[CrossRef](#)]
6. Iwamoto, H.; Ehara, M.; Akaki, M.; Kuwahara, H. Magnetoelectric property in 3d transition metal oxide with tetrahedral structure. *J. Phys. Conf. Ser.* **2012**, *400*, 032031. [[CrossRef](#)]
7. Caignaert, V.; Maignan, A.; Singh, K.; Simon, C.; Pralong, V.; Raveau, B.; Mitchell, J.F.; Zheng, H.; Huq, A.; Chapon, L.C. Gigantic magnetic-field-induced polarization and magnetoelectric coupling in a ferrimagnetic oxide $\text{CaBaCo}_4\text{O}_7$. *Phys. Rev. B* **2013**, *88*, 174403. [[CrossRef](#)]
8. Singh, K.; Caignaert, V.; Chapon, L.C.; Pralong, V.; Raveau, B.; Maignan, A. Spin-assisted ferroelectricity in ferrimagnetic $\text{CaBaCo}_4\text{O}_7$. *Phys. Rev. B* **2012**, *86*, 024410. [[CrossRef](#)]
9. Johnson, R.D.; Cao, K.; Giustino, F.; Radaelli, P.G. $\text{CaBaCo}_4\text{O}_7$: A ferrimagnetic pyroelectric. *Phys. Rev. B* **2014**, *90*, 045129. [[CrossRef](#)]
10. Omi, T.; Watanabe, Y.; Abe, N.; Sagayama, H.; Nakao, A.; Munakata, K.; Tokunaga, Y.; Arima, T. Antiferromagnetic-to-ferrimagnetic phase transition with large electric-polarization change in a frustrated polar magnet $\text{CaBaCo}_4\text{O}_7$. *Phys. Rev. B* **2021**, *103*, 18441. [[CrossRef](#)]
11. Seikh, M.M.; Kundu, A.K.; Caignaert, V.; Raveau, B. Gigantic effect of iron doping upon magnetism in the 114 magnetoelectric $\text{CaBaCo}_4\text{O}_7$. *J. Alloys Compd.* **2016**, *656*, 166–171. [[CrossRef](#)]
12. Fishman, R.S.; Bordács, S.; Kocsis, V.; Kézsmárki, I.; Viirók, J.; Nagel, U.; Rööm, T.; Puri, A.; Zeitler, U.; Tokunaga, Y.; et al. Competing exchange interactions in multiferroic and ferrimagnetic $\text{CaBaCo}_4\text{O}_7$. *Phys. Rev. B* **2017**, *95*, 024423. [[CrossRef](#)]
13. Fiebig, M.; Lottermoser, T.; Meier, D.; Trassin, M. The evolution of multiferroics. *Nat. Rev. Mater.* **2016**, *1*, 16046. [[CrossRef](#)]
14. Sekhar, C.D.; Das, A.K.; Das, A.; Venimadhav, A. Ferroelectricity in $\text{CaBaCo}_4\text{O}_7$ by light non magnetic Zn doping. *J. Phys. Condens. Matter* **2020**, *32*, 385802. [[CrossRef](#)]

15. Kazei, Z.A.; Snegirev, V.V.; Vorobev, G.P.; Popov, Y.F.; Vyalykh, D.K.; Kozeeva, L.P.; Kameneva, M.Y. Elastic, magnetic, and magnetoelectric properties of the CaBaCo₄O₇ multiferroic. *J. Exp. Theor. Phys.* **2016**, *123*, 1025–1034. [[CrossRef](#)]
16. Gen, M.; Miyake, A.; Yagiuchi, H.; Watanabe, Y.; Ikeda, A.; Matsuda, Y.H.; Tokunaga, M.; Arima, T.; Tokunaga, Y. Enhancement of giant magnetoelectric effect in Ni-doped CaBaCo₄O₇. *Phys. Rev. B* **2022**, *105*, 214412. [[CrossRef](#)]
17. Sarkar, T.; Seikh, M.M.; Pralong, V.; Caignaert, V.; Raveau, B. Magnetism of the 114 orthorhombic charge ordered CaBaCo₄O₇ doped with Zn or Ga: A spectacular valency effect. *J. Mater. Chem.* **2012**, *22*, 18043–18050. [[CrossRef](#)]
18. Oda, R.; Kajihara, R.; Nishina, K.; Akaki, M.; Kuroe, H.; Kuwahara, H. Impurity Substitution Effect on Magnetoelectric Properties of CaBaCo₄O₇ Crystals. *Phys. Proc.* **2015**, *75*, 303–308. .. [[CrossRef](#)]
19. Seikh, M.M.; Caignaert, V.; Suard, E.; Meher, P.; Maignan, A.; Raveau, B. Closely related magnetic and dielectric transitions in the 114 magnetoelectric Zn-doped CaBaCo₄O₇. *J. Appl. Phys.* **2014**, *116*, 244106. [[CrossRef](#)]
20. Hollmann, N.; Valldor, M.; Wu, H.; Hu, Z.; Qureshi, N.; Willers, T.; Chin, Y.-Y.; Cezar, J.C.; Tanaka, A.; Brookes, N.B.; et al. Orbital occupation and magnetism of tetrahedrally coordinated iron in CaBaFe₄O₇. *Phys. Rev. B* **2011**, *83*, 180405. [[CrossRef](#)]
21. Zou, Y.; Qu, Z.; Zhang, L.; Ning, W.; Ling, L.; Pi, L.; Zhang, Y. The effect of Al doping on the structure and magnetism in cobaltite CaBaCo₄O₇. *J. Alloys Compd.* **2013**, *576*, 1–4. [[CrossRef](#)]
22. Bhattacharya, S.; Das, R.; Kundu, A.K.; Seikh, M.M. High sensitivity of nickel doping upon magnetism in the 114 magnetoelectric CaBaCo₄O₇. *J. Magn. Magn. Mater.* **2022**, *557*, 169466. [[CrossRef](#)]
23. Ruan, C.L.; Yun, Z.Q.; Hu, J.Y.; Zhang, X.; Wang, S.G.; Dai, Z.X.; Zheng, G.H.; Ma, Y.Q. Magnetic entropy change CaBaCo₄O₇ compound by Al and Ni substitution. *J. Mater. Sci. Mater. Electr.* **2022**, *33*, 26881. [[CrossRef](#)]
24. Zhou, J.; Wang, Y.Q.; Gong, G.; Duan, Y.; Zuo, Y.; Su, Y. The structure, magnetic and dielectric properties of the CaBaCo_{4-x}Ni_xO₇ (0 < x < 0.1) compounds. *Ceram. Int.* **2023**, *49*, 8576–8582. [[CrossRef](#)]
25. Raveau, B.; Caignaert, V.; Pralong, V.; Pelloquin, D.; Maignan, A. A Series of Novel Mixed Valent Ferrimagnetic Oxides with a TC up to 270 K: Ca_{1-x}Y_xBaFe₄O₇. *Chem. Mater.* **2008**, *20*, 6295–6297. [[CrossRef](#)]
26. Seikh, M.M.; Pralong, V.; Caignaert, V.; Raveau, B. Local Melting of Charge Ordering in CaBaCo₄O₇ by Sr-Doping. *ZAAC* **2014**, *640*, 1141–1146. [[CrossRef](#)]
27. Katsura, H.; Nagaosa, N.; Balatsky, D.V. Spin Current and Magnetoelectric Effect in Noncollinear Magnets. *Phys. Rev. Lett.* **2005**, *95*, 057205. [[CrossRef](#)] [[PubMed](#)]
28. Yamasaki, Y.; Miyasaka, S.; Kaneko, Y.; He, J.-P.; Arima, T.; Tokura, Y. Magnetic Reversal of the Ferroelectric Polarization in a Multiferroic Spinel Oxide. *Phys. Rev. Lett.* **2006**, *96*, 207204. [[CrossRef](#)] [[PubMed](#)]
29. Tserkovnikov, Y.A. Decoupling of chains of equations for two-time Green's functions. *Teor. Mat. Fiz.* **1971**, *7*, 511. [[CrossRef](#)]
30. Cuartero, V.; Blasco, J.; Subias, G.; Garcia, J.; Rodriguez-Velamazán, J.A.; Ritter, C. CaBaCo_{4-x}M_xO₇ (M = Fe, Zn). *Inorg. Chem.* **2018**, *57*, 3360–3370. [[CrossRef](#)]
31. Wang, M.; Wang, Y.; Gong, G.; Li, Z.; Duan, Y.; Zuo, Y.; Wei, M.; Su, Y. Influence of Mn and Ni ions doping on the magnetization and dielectric properties of the CaBaCo₄O₇ compound. *J. Magn. Magn. Mater.* **2024**, *597*, 171991. [[CrossRef](#)]
32. Sekhar, C.D.; Das, A.K.; Singh, R.; Das, A.; Giovannetti, G.; Khomskii, D.; Venimadhav, A. Switching from pyroelectric to ferroelectric order in Ni doped CaBaCo₄O₇. *Phys. Rev. B* **2017**, *96*, 134413. [[CrossRef](#)]

Disclaimer/Publisher's Note: The statements, opinions and data contained in all publications are solely those of the individual author(s) and contributor(s) and not of MDPI and/or the editor(s). MDPI and/or the editor(s) disclaim responsibility for any injury to people or property resulting from any ideas, methods, instructions or products referred to in the content.